

# U-shape Transformer for Underwater Image Enhancement

Lintao Peng

Chunli Zhu

Liheng Bian \*

Beijing Institute of Technology

## Abstract

The light absorption and scattering of underwater impurities lead to poor underwater imaging quality. The existing data-driven based underwater image enhancement (UIE) techniques suffer from the lack of a large-scale dataset containing various underwater scenes and high-fidelity reference images. Besides, the inconsistent attenuation in different color channels and space areas is not fully considered for boosted enhancement. In this work, we constructed a large-scale underwater image (LSUI) dataset including 5004 image pairs, and reported an U-shape Transformer network where the transformer model is for the first time introduced to the UIE task. The U-shape Transformer is integrated with a channel-wise multi-scale feature fusion transformer (CMSFFT) module and a spatial-wise global feature modeling transformer (SGFMT) module, which reinforce the network's attention to the color channels and space areas with more serious attenuation. Meanwhile, in order to further improve the contrast and saturation, a novel loss function combining RGB, LAB and LCH color spaces is designed following the human vision principle. The extensive experiments on available datasets validate the state-of-the-art performance of the reported technique with more than 2dB superiority. The dataset and demo code are made available for non-commercial use.

## 1. Introduction

Underwater Image Enhancement (UIE) technology [38, 46] is essential for obtaining underwater images and investigating the underwater environment, which has wide applications in ocean exploration, biology, archaeology, underwater robots [19] and among other fields. However, underwater images frequently have problematic issues, such as color casts, color artifacts and blurred details [39]. Those issues could be explained by the strong absorption and scattering effect on light, which are caused by dissolved impurities and suspended matter in the medium (water). Therefore, UIE-related innovations are of great significance in

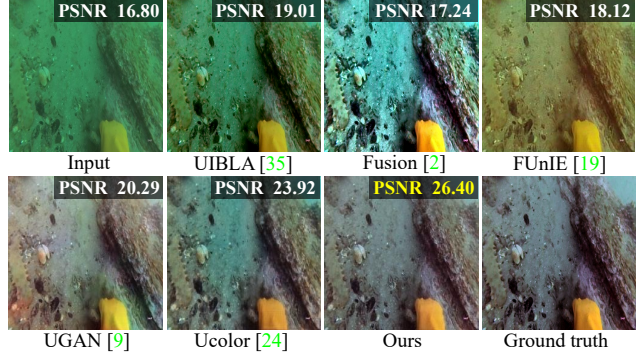


Figure 1. Compared with the existing UIE methods, the image produced by our U-shape Transformer has the highest PSNR [23] score and best visual quality.

improving the visual quality and merit of images in accurately understanding the underwater world.

In general, the existing UIE methods can be categorized into three types, which are physical model-based, visual prior-based and data-driven methods, respectively. Among them, visual prior-based UIE methods [2, 11, 13, 17, 18, 29] mainly concentrated on improving the visual quality of underwater images by modifying pixel values from the perspectives of contrast, brightness and saturation. Nevertheless, the ignorance of the physical degradation process limits the improvement of enhancement quality. In addition, physical-model based UIE methods [5, 7, 8, 12, 15, 27, 30, 35, 44] mainly focus on the accurate estimation of medium transmission. With the estimated medium transmission and other key underwater imaging parameters such as the homogeneous background light, a clean image can be obtained by reversing a physical underwater imaging model. However, the performance of physical model-based UIE is restricted to complicated and diverse real-world underwater scenes. That is because, (1) *model hypothesis is not always plausible with complicated and dynamic underwater environment*; (2) *evaluating multiple parameters simultaneously is challenging*. More recently, as to the data-driven methods [1, 9, 10, 14, 19, 24, 26, 28, 31, 39–41, 45], which could be regarded as deep learning technologies in UIE domain, exhibit impressive performance on UIE task. How-

\*Corresponding author: Bian@bit.edu.cn

ever, the existing underwater datasets more-or-less have the disadvantages, such as a small number of images, few underwater scenes, or even not real-world scenarios, which limits the performance of the data-driven UIE method. Besides, the inconsistent attenuation of the underwater images in different color channels and space areas have not been unified in one framework.

In this work, we first built a large scale underwater image (LSUI) dataset, which covers more abundant underwater scenes and better visual quality reference images than existing underwater datasets [1, 26, 31, 32]. The dataset contains 5004 real-world underwater images, and the corresponding clear images are generated as comparison references. Furthermore, with the prior knowledge that the attenuation of different color channels and space areas in underwater images is inconsistent, we designed a channel-wise multi-scale feature fusion transformer (CMSFFT) and a spatial-wise global feature modeling transformer (SGFMT) based on the attention mechanism, and embedded them in our U-shape Transformer which is designed based on [20]. Moreover, a multi-scale gradient flow mechanism [22] is utilized to guarantee the stable training process, whilst a multi-color space loss function is constructed with the RGB, LAB and LCH color space in accordance with the human eye's cognition. Fig. 7 shows the result of our UIE method and some comparison UIE methods, and the main contributions of this paper can be summarized as follows:

- We reported a novel U-shape Transformer dealing with the UIE task, in which the designed channel-wise and spatial-wise attention mechanism enables to effectively remove color artifacts and casts.
- We designed a novel multi-color space loss function combining the RGB, LCH and LAB color-space features, which further improves the contrast and saturation of output images.
- We released a large-scale underwater dataset containing 5004 image pairs, which facilitates further development of underwater imaging techniques.

## 2. Related work

### 2.1. Data-driven UIE Methods

As we mentioned the pros and cons of physical model-based and visual prior-based UIE methods in section 1, this part concerns only data-driven UIE methods.

Current data-driven UIE methods can be divided into two main technical routes, (1) *designing an end-to-end module* (2) *utilizing deep models directly to estimate physical parameters, and then restore the clean image based on the degradation model*. To alleviate the need for real-world underwater paired training data, Li et al. [31] proposed a Wa-

terGAN to generate underwater-like images from in-air images and depth maps in an unsupervised manner, in which the generated dataset is further used to train the WaterGAN. Moreover, [28] exhibited a weakly supervised underwater color transmission model based on CycleGAN [49]. Benefiting from the adversarial network architecture and multiple loss functions, that network can be trained using unpaired underwater images, which refines the adaptability of the network model to underwater scenes. However, images in the training dataset used by the above methods are not matched real underwater images, which leads to limited enhancement effects of the above methods in diverse real-world underwater scenes. Recently, Li et al. [26] proposed a gated fusion network named WaterNet, which uses gamma-corrected images, contrast-improved images, and white-balanced images as the inputs to enhance underwater images. Yang et al. [47] proposed a conditional generative adversarial network (cGAN) to improve the perceptual quality of underwater images.

The methods mentioned above usually use existing deep neural networks for general purposes directly on UIE tasks and neglect the unique characteristics of underwater imaging. For example, [28] directly used the CycleGAN [49] network structure, and [26] adopted a simple multi-scale convolutional network. Other models such as UGAN [9], WaterGAN [31] and cGAN [47], they still inherited the disadvantage of GAN-based models, which produces unstable enhancement results. In addition, Ucolor [24] combined the underwater physical imaging model and designed a medium transmission guided model to reinforce the network's response to areas with more severe quality degradation, which could improve the visual quality of the network output to a certain extent. However, physical models sometimes failed with varied underwater environments.

From above, our proposed network aims at generating high visual quality underwater images by properly accounting the inconsistent attenuation characteristics of underwater images in different color channels and space areas.

### 2.2. Underwater Image Datasets

The sophisticated and dynamic underwater environment results in extreme difficulties in the collection of matched underwater image training data in real-world underwater scenes. Present datasets can be classified into two types, they are, (1) Non-reference datasets. Liu et al. [32] proposed RUIE dataset, which encompasses varied underwater lighting, depth of field, blurriness and color cast scenes. Akkaynak et al. [1] published a non-reference underwater dataset with a standard color comparison chart. Those datasets, however, cannot be used for end-to-end training for lacking matched clear reference underwater images. (2) Full-reference datasets. Li et al. [31] presented an unsupervised network dubbed WaterGAN to produce underwater-

like images using in-air images and depth maps. Similarly, Fabbri et al. [9] used CycleGAN to generate distorted images from clean underwater images based on weakly supervised distribution transfer. However, these methods rely heavily on training samples, which is easy to produce artifacts that are out of reality and unnatural. Li et al. [26] constructed a real UIE benchmark UIEB, including 890 images pairs, in which reference images were hand-crafted using the existing optimal UIE methods. Although those images are authentic and reliable, the number, content and coverage of underwater scenes are limited. In contrast, our LSUI dataset contains 5004 real underwater images pairs, which has abundant underwater environments and higher visual quality references.

### 3. Proposed dataset and method

#### 3.1. LSUI Dataset

**Data Collection.** We have collected 8018 underwater images, which are sourced from Bubble Vision<sup>1</sup>, BIOS<sup>2</sup> and existing datasets [1, 9, 26, 31, 32]. Real underwater images with rich water scenes, water types, lighting conditions and target categories, are selected to the extent possible, for further generating clear reference images.

**Reference Image Generation.** Inspired by ensemble learning [36] that multiple weak classifiers could form a strong one, we use 17 existing optimal UIE methods [2, 5, 7, 8, 10–12, 19, 27, 28, 30, 31, 35, 40, 41, 45] to process the collected underwater images successively. Moreover, a commercial software Dive+<sup>3</sup> is used to make the alternative reference images. Accordingly, a set with  $18 * 8018$  images is generated for the next-step optimal reference dataset selection.

In order to reduce the number of images that need to be selected manually, non-reference metrics UIQM [34] and UCIQE [48] are adopted to score all generated images with equal weights. Then, the top-three reference images of each original one form a set with the size  $3 * 8018$ . Considering individual differences, 10 volunteers were invited to rate images with a score from 0 to 10, where the higher score represents the more contentedness. Note here original image would also be provided to volunteers. With subjective scores from 10 volunteers, and objectively scores from UIQM and UCIQE, each reference picture could obtain 12 scores. Here, the manual scores were normalized between 0 and 1, for further summing with UIQM and UCIQE. The top-one reference image was chosen with the highest summation. In addition, images with the highest summation lower than 8 have been removed from the dataset. Eventually, our LSUI dataset contains 5004 pair of images.

<sup>1</sup><https://www.naturefootage.com/stock-video/ocean-underwater-video>

<sup>2</sup><https://coral.bios.edu/in-water-validation/>

<sup>3</sup><http://dive.plus/>

### 3.2. U-shape Transformer

#### 3.2.1 Overall Architecture

The overall architecture of the U-shape Transformer is shown as Fig. 8, which includes a CMSFFT & SGFMT based generator and a discriminator.

In the generator, (1) Encoding: Except being directly input to the network, the original image will be downsampled three times respectively. Then after  $1*1$  convolution, the three scale feature maps are input into the corresponding scale convolution block. The outputs of four convolutional blocks are the inputs of the CMSFFT and SGFMT; (2) Decoding: After feature remapping, the SGFMT output is directly sent to the first convolutional block. Meanwhile, four convolutional blocks with varied scales will receive the four outputs from CMSFFT.

In the discriminator, the input of the four convolutional blocks includes: the feature map output by its own upper layer, the feature map of the corresponding size from the decoding part and the feature map generated by  $1*1$  convolution after downsampling to the corresponding size using the reference image. With the described multi-scale connections, the gradient flow can flow freely on multiple scales between the generator and the discriminator, such that a stable training process could be obtained, details of the generated images could be enriched. The detailed structure of SGFMT and CMSFFT in the network will be described in the following two subsections.

#### 3.2.2 SGFMT

The SGFMT (as shown in Fig. 9) is used to replace the original bottleneck layer of the generator, which can assist the network to model the global information and reinforce the network’s attention on severely degraded parts. Assuming the size of the input feature map is  $F_{in} \in \mathbb{R}^{\frac{H}{16} * \frac{W}{16} * C}$ . For the expected one-dimensional sequence of the transformer, linear projection is used to stretch the two-dimensional feature map into a feature sequence  $S_{in} \in \mathbb{R}^{\frac{HW}{256} * C}$ . For preserving the valued position information of each region, learnable position embedding is merged directly, which can be expressed as,

$$S_{in} = W * F_{in} + PE, \quad (1)$$

where  $W * F_i$  represents a linear projection operation, PE represents a position embedding operation.

Then we input the feature sequence  $S_{in}$  to the transformer block, which contains 4 standard transformer layers [42]. Each transformer layer contains a multi-head attention block (MHA) and a feed-forward network (FFN). The FFN includes a normalization layer and a fully connected layer. The output of the  $l$ -th ( $l \in [1, 2, \dots, l]$ ) layer

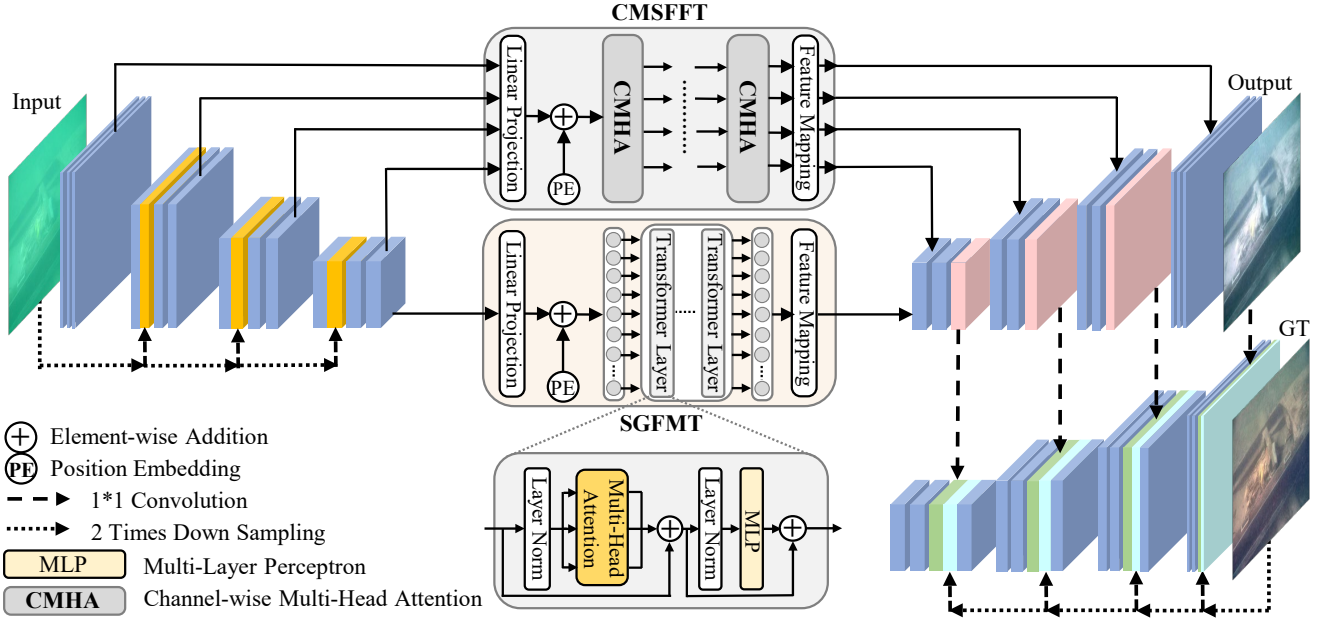


Figure 2. The network structure of the reported U-shape Transformer. CMSFFT and SGFMT reinforce the network’s attention to the more severely attenuated color channels and spatial regions. The multi-scale connections of the generator and the discriminator make the gradient flow freely between the generator and the discriminator, therefore making the training process more stable.

in the transformer block can be calculated by,

$$S'_l = \text{MHA}(\text{LN}(S_{l-1})) + S_{l-1} \quad (2)$$

$$S_l = \text{FFN}(\text{LN}(S'_l)) + S'_l, \quad (3)$$

where LN represents layer normalization, and  $S_l$  represents the output sequence of the  $l$ -th layer in the transformer block. The output feature sequence of the last transformer block is  $S_l \in \mathbb{R}^{\frac{HW}{256} \times C}$ , which is restored to the feature map of  $F_{out} \in \mathbb{R}^{\frac{H}{16} \times \frac{W}{16} \times C}$  after feature remapping.

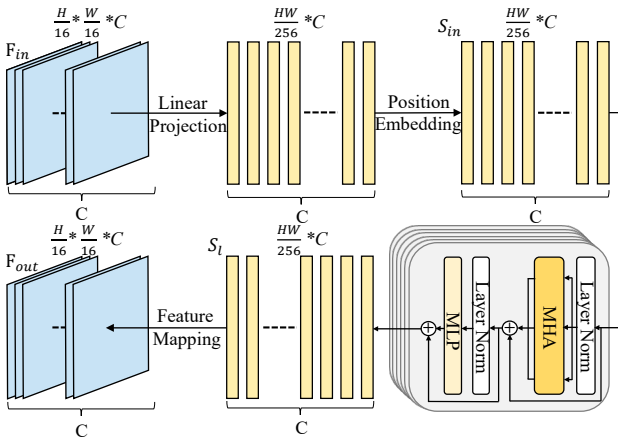


Figure 3. Data flow diagram of the SGFMT module.

### 3.2.3 CMSFFT

To reinforce the network’s attention on the more serious attenuation color channels, inspired by [43], we designed the CMSFFT block to replace the skip connection of the original generator’s encoding-decoding architecture (Fig.10), which consists of the following three parts.

**Multi-Scale Feature Encoding.** The inputs of CMSFFT are the feature maps  $F_i \in \mathbb{R}^{\frac{H}{2^i} \times \frac{W}{2^i} \times C_i}$  ( $i = 0, 1, 2, 3$ ) with different scales. Differs from the linear projection in Vit [6] which is applied directly on the partitioned original image, we use convolution kernels with related filter size  $\frac{P}{2^i} \times \frac{P}{2^i}$  ( $i = 0, 1, 2, 3$ ) and step size  $\frac{P}{2^i}$  ( $i = 0, 1, 2, 3$ ), to conduct linear projection on feature maps with varied scales. In this work,  $P$  is set as 32. After that, four feature sequence  $S_i \in \mathbb{R}^{d \times C_i}$  ( $i = 1, 2, 3, 4$ ) could be obtained, where  $d \in \frac{HW}{P^2}$ . Those four convolution kernels divide feature maps into the same number of blocks, while the number of channels  $C_i$  ( $i = 1, 2, 3, 4$ ) remains unchanged. Then, four query vectors  $Q_i \in \mathbb{R}^{d \times C_i}$  ( $i = 1, 2, 3, 4$ ),  $K \in \mathbb{R}^{d \times C}$  and  $V \in \mathbb{R}^{d \times C}$  can be obtained by Eq.(4).

$$Q_i = S_i W_{Q_i} \quad K = S W_K \quad V = S W_V, \quad (4)$$

where  $W_{Q_i} \in \mathbb{R}^{d \times C_i}$  ( $i = 1, 2, 3, 4$ ),  $W_K \in \mathbb{R}^{d \times C}$  and  $W_V \in \mathbb{R}^{d \times C}$  stands for learnable weight matrices;  $S$  is generated by concatenating  $S_i \in \mathbb{R}^{d \times C_i}$  ( $i = 1, 2, 3, 4$ ) via the channel dimension, where  $C = C_1 + C_2 + C_3 + C_4$ . In



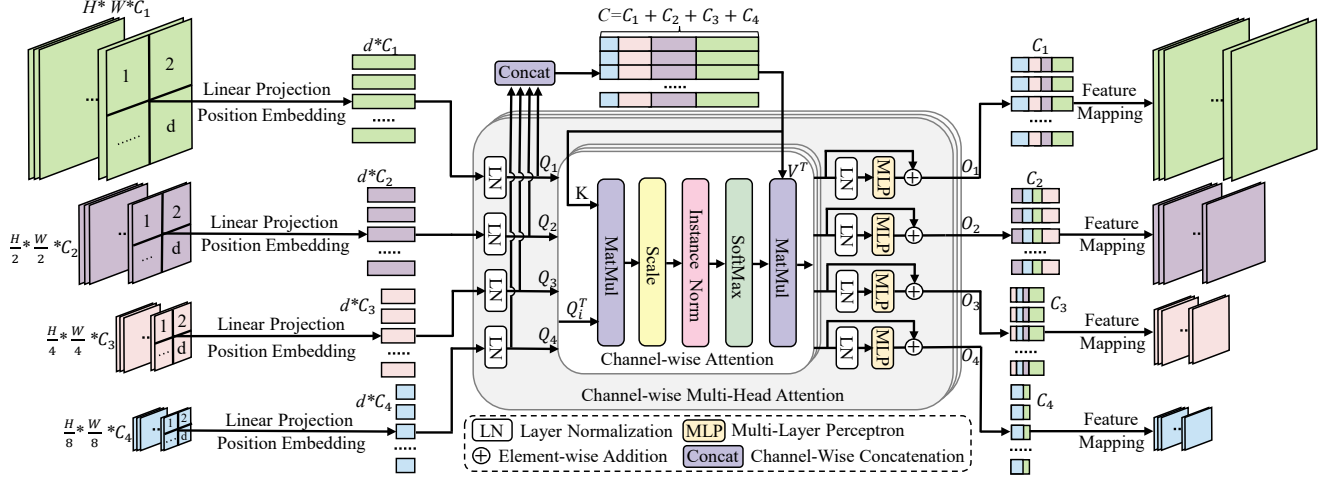


Figure 4. Detailed structure of the CMSFFT module.

this work,  $C_1$ ,  $C_2$ ,  $C_3$ , and  $C_4$  are set as 64, 128, 256, 512, respectively.

**Channel-Wise Multi-Head Attention (CMHA).** The CMHA block has six inputs, which are  $K \in \mathbb{R}^{d \times C}$ ,  $V \in \mathbb{R}^{d \times C}$  and  $Q_i \in \mathbb{R}^{d \times C_i}$  ( $i = 1, 2, 3, 4$ ). The output of channel-wise attention  $CA_i \in \mathbb{R}^{C_i \times d}$  ( $i = 1, 2, 3, 4$ ) could be obtained by,

$$CA_i = \text{SoftMax}(\text{IN}(\frac{Q_i^T K}{\sqrt{C}}))V^T, \quad (5)$$

where IN represents the instance normalization operation. This attention operation performs along the channel-axis instead of the classical patch-axis [6], which can guide the network to pay attention to channels with more severe image quality degradation. In addition, IN is used on the similarity maps to assist the gradient flow spreads smoothly.

The output of the  $i$ -th CMHA layer can be expressed as,

$$\text{CMHA}_i = (CA_i^1 + CA_i^2 + \dots + CA_i^N)/N + Q_i, \quad (6)$$

where  $N$  is the number of heads, which is set as 4 in our implementation.

**Feed-Forward Network (FFN).** Similar to the forward propagation of [6], the FFN output can be expressed as,

$$O_i = \text{CMHA}_i + \text{MLP}(\text{LN}(\text{CMHA}_i)), \quad (7)$$

where  $O_i \in \mathbb{R}^{d \times C_i}$  ( $i = 1, 2, 3, 4$ ); MLP stands for multi-layer perception. Here, The operation in Eq. (7) needs to be repeated  $l$  ( $l=4$  in this work) times in sequence to build the  $l$ -layer transformer.

Finally, feature remappings are performed on the four different output feature sequences  $O_i \in \mathbb{R}^{C_i \times d}$  ( $i = 1, 2, 3, 4$ ) to reorganize them into four feature maps  $F_i \in \mathbb{R}^{\frac{H}{2^i} \times \frac{W}{2^i} \times C_i}$  ( $i = 0, 1, 2, 3$ ), which are the input of convolutional block in the generator's decoding part.

### 3.3. Loss Function

To take advantage of the LAB and LCH color spaces' wider color gamut representation range and more accurate description of the color saturation and brightness, we designed a multi-color space loss function combining RGB, LAB and LCH color spaces to train our network. The image from RGB space is firstly converted to LAB and LCH space, and reads,

$$L^{G(x)}, A^{G(x)}, B^{G(x)} = \text{RGB2LAB}(G(x)) \quad (8)$$

$$L^y, A^y, B^y = \text{RGB2LAB}(y), \quad (9)$$

$$L^{G(x)}, C^{G(x)}, H^{G(x)} = \text{RGB2LCH}(G(x)), \quad (10)$$

$$L^y, C^y, H^y = \text{RGB2LCH}(y), \quad (11)$$

where  $x, y$  and  $G(x)$  represents the original inputs, the reference image, and the clear image output by the generator, respectively.

Loss functions in the LAB and LCH space are written as Eq.(10) and Eq.(11).

$$\begin{aligned} \text{Loss}_{\text{LAB}}(G(x), y) = E_{x,y} [ & (L^y - L^{G(x)})^2 - \\ & \sum_{i=1}^n Q(A_i^y) \log(Q(A_i^{G(x)})) - \sum_{i=1}^n Q(B_i^y) \log(Q(B_i^{G(x)})) ], \end{aligned} \quad (10)$$

$$\begin{aligned} \text{Loss}_{\text{LCH}}(G(x), y) = E_{x,y} [ & - \sum_{i=1}^n Q(L_i^y) \log(Q(L_i^{G(x)})) \\ & + (C^y - C^{G(x)})^2 + (H^y - H^{G(x)})^2 ], \end{aligned} \quad (11)$$

where  $Q$  stands for the quantization operator.

$L_2$  loss in the RGB color space  $\text{Loss}_{\text{RGB}}$  and the perceptual loss  $\text{Loss}_{\text{per}}$  [21], as well as  $\text{Loss}_{\text{LAB}}$  and  $\text{Loss}_{\text{LCH}}$  are the four loss functions for the generator.

Besides, standard GAN loss function is introduced for minimizing the loss between generated and reference pictures, and written as,

$$L_{GAN}(G, D) = E_y[\log D(y)] + E_x[\log(1 - D(G(x)))], \quad (12)$$

where  $D$  represents the discriminator.  $D$  aims at maximizing  $L_{GAN}(G, D)$ , to accurately distinguish the generated image from the reference image. And the goal of generator  $G$  is to minimize the loss between generated pictures and reference pictures.

Then, the final loss function is expressed as,

$$\begin{aligned} G^* = \arg \min_G \max_D L_{GAN}(G, D) &+ \alpha Loss_{LAB}(G(x), y) \\ &+ \beta Loss_{LCH}(G(x), y) + \gamma Loss_{RGB}(G(x), y) \\ &+ \mu Loss_{per}(G(x), y), \end{aligned} \quad (13)$$

where  $\alpha, \beta, \gamma, \mu$  are hyperparameters, which are set as 0.001, 1, 0.1, 100, respectively, with numerous experiments.

## 4. Experiments

### 4.1. Implementation Details

The LSUI dataset was randomly divided as Train-L (4500 images) and Test-L504 (504 images) for training and testing, respectively. The training set was enhanced by cropping, rotating and flipping the existing images. All images were adjusted to a fixed size (256\*256) when input to the network, and the pixel value will be normalized to [0,1].

We use python and pytorch framework via NVIDIA RTX3090 on Ubuntu20 to implement the U-shape Transformer. Adam optimization algorithm is utilized for the total of 800 epochs training with batchsize set as 6. The initial learning rate is set as 0.0005 and 0.0002 for the first 600 epochs and the last 200 epochs, respectively. Besides, the learning rate decreased 20% every 40 epochs. For  $Loss_{RGB}$ ,  $L_2$  loss is used for the first 600 epochs, and  $L_1$  loss is used for the last 200 epochs.

### 4.2. Experiment Settings

**Benchmarks.** Besides Train-L, the second training set Train-U contains 800 pairs of underwater images from UIEB [26] and 1,250 synthetic underwater images from [25]; the third training set Train-E contains the paired training images in the EUVP [19] dataset. Testing datasets are categorized into two types, (1) full-reference testing dataset: Test-L504 and Test-U90 (remaining 90 pairs in UIEB); (2) non-reference testing dataset: Test-U60 and SQUID. Here, Test-U60 includes 60 non-reference images in UIEB; 16 pictures from SQUID [1] forms the second non-reference testing dataset.

**Compared Methods.** We compare U-shape Transformer with 10 UIE methods to verify our performance superiority. It includes two physical-based models (UIBLA [35],

UDCP [8]), three visual prior-based methods (Fusion [2], retinex based [11], RGHS [17]), and five data-driven methods (WaterNet [26], FUnIE [19], UGAN [9], UIE-DAL [41], Ucolor [24]).

**Evaluation Metrics.** For the testing dataset with reference images, we conducted full-reference evaluations using PSNR [23] and SSIM [16] metrics. Those two metrics reflect the proximity to the reference, where a higher PSNR value represents closer image content, and a higher SSIM value reflects a more similar structure and texture.

For images in the non-reference testing dataset, non-reference evaluation metrics UCIQE [48] and UIQM [34] are employed, in which higher UCIQE or UIQM score suggests better human visual perception. For UCIQE and UIQM cannot accurately measure the performance in some cases [26] [3], we also conducted an user survey following [24], which results are stated as ‘‘perception score (PS)’’. In the user survey, 10 volunteers with image processing background were invited to score the enhancement results. The integral score from 1 to 5 represents image quality from the worst to the best, which criterion is from color deviation, artifacts, natural looking, and contrast & visibility. Each image’s final PS score is the average value of all volunteers. Moreover, NIQE [33], which lower value represents a higher visual quality, is also adopted as the metrics.

### 4.3. Dataset Evaluation

The effectiveness of LSUI is evaluated by retraining the compared methods (U-net [37], UGAN [9] and U-shape Transformer) on Train-L, Train-U and Train-E. The trained network was tested on Test-L504 and Test-U90. As shown in Tab.1, the model trained on our dataset is the best of PSNR and SSIM. It could be explained that LSUI contains richer underwater scenes and better visual quality reference images than existing underwater image datasets, which can improve the enhancement and generalization ability of the tested network. The visual comparisons can be found in the supplementary material.

Table 1. Dataset evaluation results. The highest PSNR and SSIM scores are marked in red.

Methods	Training Data	Test-U90		TestL-504	
		PSNR	SSIM	PSNR	SSIM
U-net [37]	Train-U	17.07	0.76	19.19	0.79
	Train-E	17.46	0.76	19.45	0.78
	Ours	20.14	0.81	20.89	0.82
UGAN [9]	Train-U	20.71	0.82	19.89	0.79
	Train-E	20.72	0.82	19.82	0.78
	Ours	21.56	0.83	21.74	0.84
Ours	Train-U	21.25	0.84	22.87	0.85
	Train-E	21.75	0.86	23.01	0.87
	Ours	22.91	0.91	24.16	0.93

#### 4.4. Network Architecture Evaluation

**Full-Reference Evaluation.** The Test-L504 and Test-U90 datasets were used for evaluation. The statistical results and visual comparisons are summarized in Tab. 2 and Fig. 11. For the 5 deep learning based UIE methods, we used the code and pre-training weights provided by the authors.

Table 2. Quantitative comparison among different UIE methods on the full-reference testing set. The highest scores are marked in red.

Methods	Test-L504		Test-U90	
	PSNR	SSIM	PSNR	SSIM
UIBLA [35]	13.54	0.71	15.78	0.73
UDCP [8]	11.89	0.59	13.81	0.69
Fusion [2]	17.48	0.79	19.04	0.82
Retinex based [11]	13.89	0.74	14.01	0.72
RGHS [17]	14.21	0.78	14.57	0.79
WaterNet [26]	17.73	0.82	19.81	0.86
FUnIE [19]	19.37	0.84	19.45	0.86
UGAN [9]	19.79	0.78	20.68	0.84
UIE-DAL [41]	17.45	0.79	16.37	0.78
Ucolor [24]	22.91	0.89	20.78	0.87
Ours	<b>24.16</b>	<b>0.93</b>	<b>22.91</b>	<b>0.91</b>

As in Tab.2, our U-shape Transformer demonstrates the best performance for both PSNR and SSIM metrics. The potential limitations of the poor performance of the 5 data-driven methods are analyzed as follows. FUnIE [19] aims at achieving fast, lightweight and fewer parameter models, thereby it is easy to reach the performance bottleneck on complex and distorted testing samples. UGAN [9] and UIE-DAL [41] ignore the inconsistent characteristics of the underwater images. Although Ucolor [24] also introduced the concept of multi-color space, it simply adds them to the network’s encoding part, which cannot fully utilize the advan-

tages of multi-color space.

The visual comparisons shown in Fig. 11 reveal that enhancement results of our method are the closest to the reference image, which has fewer color artifacts and high-fidelity object areas. Five selected methods tend to produce color artifacts that deviated from the original color of the object. Among the methods, Fusion [2] exhibits severe color artifacts. Retinex based [11] could improve the image contrast to a certain extent, but cannot remove the color casts and color artifacts effectively. The enhancement result of FUnIE [19] is yellowish overall. Although UGAN [9] and Ucolor [26] could provide relatively good color appearance, they are often affected by local over-enhancement, and there are still some color casts in the result.

**Non-reference Evaluation.** The Test-U60 and SQUID datasets were utilized for the non-reference evaluation, in which statistical results and visual comparisons are shown in Tab. 3 and Fig. 12.

As in Tab. 3, our method achieved the highest scores on PS and NIQE metrics, which confirmed the initial idea to contemplate the human eye’s color perception and better generalization ability to varied real-world underwater scenes. Note that UCIQE and UIQM of all deep learning-based UIE methods are weaker than physical model-based or visual prior-based, also reported in [24]. Those two metrics are of valuable reference, but cannot as absolute justifications [26] [3], for they are non-sensitive to color artifacts & casts and biased to some features.

UGAN and Ucolor are selected for visual comparison according to previous results, as in Fig. 12, where UGAN has obvious color artifacts in some local areas and Ucolor has an obvious color cast. That is due to the architecture of UGAN and Ucolor ignoring the inconsistent attenuation characteristics of underwater image on different image areas and color channels, respectively. In our method, the reported CMSFFT and SGFMT modules could reinforce

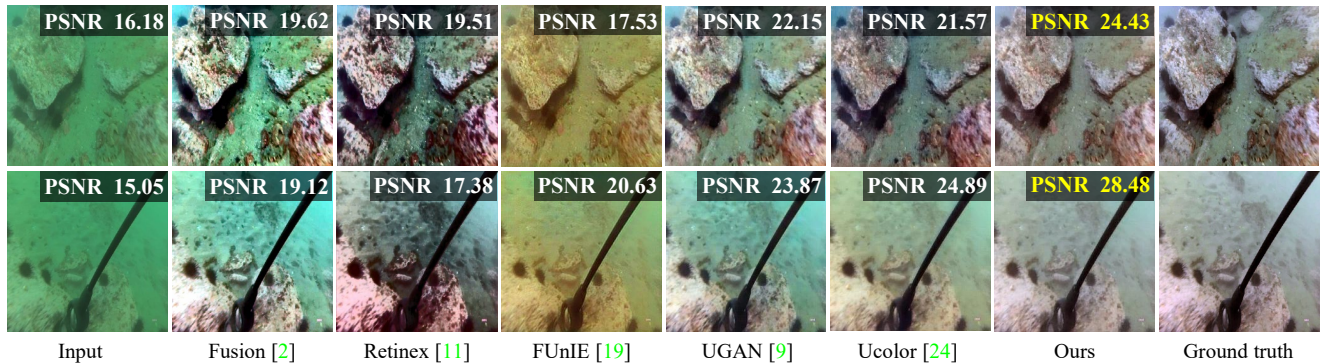


Figure 5. Visual comparison of enhancement results sampled from the Test-L504 dataset. From left to right are raw images, results of Fusion [2], Retinex based [11], FUnIE [19], UGAN [9], Ucolor [24], our U-shape Transformer and the reference image (recognized as ground truth (GT)). More examples can be found in the supplementary material.

Table 3. Quantitative comparison among different UIE methods on the non-reference testing set. The highest scores are marked in red.

Methods	Test-U60				SQUID			
	PS $\uparrow$	UIQM $\uparrow$	UCIQE $\uparrow$	NIQE $\downarrow$	PS $\uparrow$	UIQM $\uparrow$	UCIQE $\uparrow$	NIQE $\downarrow$
input	1.46	0.82	0.45	7.16	1.23	0.81	0.43	4.93
UIBLA [35]	2.18	1.21	0.60	6.13	2.45	0.96	0.52	4.43
UDCP [8]	2.01	1.03	0.57	5.94	2.57	1.13	0.51	4.47
Fusion [2]	2.12	<b>1.23</b>	0.61	4.96	2.89	<b>1.29</b>	0.61	5.01
Retinex based [11]	2.04	0.94	0.69	4.95	2.33	1.01	0.66	4.86
RGHS [17]	2.45	0.66	0.71	4.82	2.67	0.82	<b>0.73</b>	4.54
WaterNet [26]	3.23	0.92	0.51	6.03	2.72	0.98	0.51	4.75
FUnIE [19]	3.12	1.03	0.54	6.12	2.65	0.98	0.51	4.67
UGAN [9]	3.64	0.86	0.57	6.74	2.79	0.90	0.58	4.56
UIE-DAL [41]	2.03	0.72	0.54	4.99	2.21	0.79	0.57	4.88
Ucolor [24]	3.71	0.84	0.53	6.21	2.82	0.82	0.51	4.32
Ours	<b>3.91</b>	0.85	<b>0.73</b>	<b>4.74</b>	<b>3.23</b>	0.89	0.67	<b>4.24</b>

the network’s attention to the color channels and spatial regions with serious attenuation, therefore obtaining high visual quality enhancement results without color artifacts and color casts.

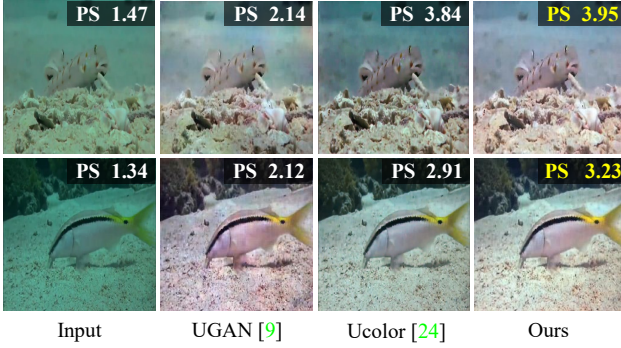


Figure 6. Visual comparison sampled from the Test-U60 dataset. UGAN [9] and Ucolor [24] are selected for visual comparison considering their performance in full-reference experiment. More examples can be found in the supplementary material.

#### 4.5. Ablation Study

To prove the effectiveness of each component, we conduct a series of ablation studies on the Test-L504 and Test-U90. Four factors are considered including the CMSFFT, the SGFMT, the multi-scale gradient flow mechanism (MSG) and the multi-color space loss function (MCSL).

Experiments are all trained by Train-L. Statistical results are shown in Tab. 4, in which baseline model (BL) refers to [20], full models is the complete U-shape Transformer. In Tab. 4, our full model achieves the best quantitative performance on the two testing dataset, which reflects the effectiveness of the combination of CMSFFT, SGFMT, MSG and MCSL modules. Compared with the

BL model, BL+CMSFFT, BL+SGMFT, BL+MSG and BL+MCSL have achieved better results, which proves the effectiveness of each module.

Table 4. Statistical results of ablation study on the Test-L504 and the Test-U90. The highest scores are marked in red.

Models	Test-L504		Test-U90	
	PSNR	SSIM	PSNR	SSIM
BL	19.34	0.79	19.36	0.81
BL+CMSFFT	22.47	0.88	21.72	0.86
BL+SGFMT	21.78	0.86	21.36	0.87
BL+MSG	20.11	0.82	21.24	0.85
BL+MCSL	21.51	0.82	20.16	0.81
Full Model	<b>24.16</b>	<b>0.93</b>	<b>22.91</b>	<b>0.91</b>

## 5. Conclusions

In this work, we released the LSUI dataset which is the largest real-world underwater dataset with high-fidelity reference images. Besides, we reported an U-shape Transformer network for state-of-the-art enhancement. The network’s CMSFFT and SGFMT modules could solve the inconsistent attenuation issue of underwater images in different color channels and space regions, which has not been considered among existing methods. Extensive experiments validate the superior ability of the network to remove color artifacts and casts. Combined with the multi-color space loss function, the contrast and saturation of output images are further improved. Nevertheless, it is impossible to collect images of all the complicated scenes such as deep-ocean low-light scenarios. Therefore, we will introduce other general enhancement techniques such as low-light boosting [4] for further improvement.



## References

- [1] Derya Akkaynak and Tali Treibitz. Sea-thru: A method for removing water from underwater images. In *CVPR*, pages 1682–1691, 2019. 1, 2, 3, 6
- [2] Cosmin Ancuti, Codruta Orniana Ancuti, Tom Haber, and Philippe Bekaert. Enhancing underwater images and videos by fusion. In *CVPR*, pages 81–88, 2012. 1, 3, 6, 7, 8, 11, 13
- [3] Dana Berman, Deborah Levy, Shai Avidan, and Tali Treibitz. Underwater single image color restoration using haze-lines and a new quantitative dataset. *IEEE TPAMI*, 43(8):2822–2837, 2021. 6, 7
- [4] Chen Chen, Qifeng Chen, Jia Xu, and Vladlen Koltun. Learning to see in the dark. In *CVPR*, pages 3291–3300, 2018. 8
- [5] John Y. Chiang and Ying-Ching Chen. Underwater image enhancement by wavelength compensation and dehazing. *IEEE TIP*, 21(4):1756–1769, 2012. 1, 3
- [6] Alexey Dosovitskiy, Lucas Beyer, Alexander Kolesnikov, Dirk Weissenborn, Xiaohua Zhai, Thomas Unterthiner, Mostafa Dehghani, Matthias Minderer, Georg Heigold, Sylvain Gelly, Jakob Uszkoreit, and Neil Houlsby. An image is worth 16x16 words: Transformers for image recognition at scale. *ArXiv*, abs/2010.11929, 2021. 4, 5
- [7] Paulo L.J. Drews, Erickson R. Nascimento, Silvia S.C. Botelho, and Mario Fernando Montenegro Campos. Underwater depth estimation and image restoration based on single images. *IEEE Comput. Graph. Appl.*, 36(2):24–35, 2016. 1, 3
- [8] P. Drews Jr, E. do Nascimento, F. Moraes, S. Botelho, and M. Campos. Transmission estimation in underwater single images. In *ICCV workshops*, pages 825–830, 2013. 1, 3, 6, 7, 8
- [9] Cameron Fabbri, Md. Jahidul Islam, and Junaed Sattar. Enhancing underwater imagery using generative adversarial networks. *ICRA*, pages 7159–7165, 2018. 1, 2, 3, 6, 7, 8, 11, 13
- [10] Xueyang Fu, Zhiwen Fan, Mei Ling, Yue Huang, and Xinghao Ding. Two-step approach for single underwater image enhancement. In *ISPACS*, pages 789–794, 2017. 1, 3
- [11] Xueyang Fu, Peixian Zhuang, Yue Huang, Yinghao Liao, Xiao-Ping Zhang, and Xinghao Ding. A retinex-based enhancing approach for single underwater image. In *ICIP*, pages 4572–4576, 2014. 1, 3, 6, 7, 8, 11, 13
- [12] Adrian Galdran, David Pardo, Artzai Picón, and Aitor Alvarez-Gila. Automatic red-channel underwater image restoration. *JVCIR*, 26:132–145, 2015. 1, 3
- [13] Ahmad Shahrizan Abdul Ghani and Nor Ashidi Mat Isa. Underwater image quality enhancement through composition of dual-intensity images and rayleigh-stretching. In *ICCE*, pages 219–220, 2014. 1
- [14] Yecai Guo, Hanyu Li, and Peixian Zhuang. Underwater image enhancement using a multiscale dense generative adversarial network. *IEEE J. OCEANIC. ENG.*, 45(3):862–870, 2019. 1
- [15] Kaiming He, Jian Sun, and Xiaoou Tang. Single image haze removal using dark channel prior. In *CVPR*, pages 1956–1963, 2009. 1
- [16] Alain Horé and Djemel Ziou. Image quality metrics: Psnr vs. ssim. In *ICPR*, pages 2366–2369, 2010. 6
- [17] Dongmei Huang, Yan Wang, Wei Song, Jean Sequeira, and Sébastien Mavromatis. Shallow-water image enhancement using relative global histogram stretching based on adaptive parameter acquisition. In *MMM*, pages 453–465. Springer, 2018. 1, 6, 7, 8
- [18] Kashif Iqbal, Michael Odetayo, Anne James, Rosalina Abdul Salam, and Abdullah Zawawi Hj Talib. Enhancing the low quality images using unsupervised colour correction method. In *IEEE Int. Conf. Syst. Man. Cybern.*, pages 1703–1709, 2010. 1
- [19] Md Jahidul Islam, Youya Xia, and Junaed Sattar. Fast underwater image enhancement for improved visual perception. *IEEE Robot. Autom. Lett.*, 5(2):3227–3234, 2020. 1, 3, 6, 7, 8, 11, 13
- [20] Phillip Isola, Jun-Yan Zhu, Tinghui Zhou, and Alexei A Efros. Image-to-image translation with conditional adversarial networks. In *CVPR*, pages 1125–1134, 2017. 2, 8
- [21] Justin Johnson, Alexandre Alahi, and Li Fei-Fei. Perceptual losses for real-time style transfer and super-resolution. In *ECCV*, 2016. 5
- [22] Animesh Karnewar and Oliver Wang. Msg-gan: Multi-scale gradients for generative adversarial networks. In *CVPR*, pages 7796–7805, 2020. 2
- [23] Jari Korhonen and Junyong You. Peak signal-to-noise ratio revisited: Is simple beautiful? In *QoMEX*, pages 37–38. IEEE, 2012. 1, 6
- [24] Chongyi Li, Saeed Anwar, Junhui Hou, Runmin Cong, Chunle Guo, and Wenqi Ren. Underwater image enhancement via medium transmission-guided multi-color space embedding. *IEEE TIP*, 30:4985–5000, 2021. 1, 2, 6, 7, 8, 11, 13
- [25] Chongyi Li, Saeed Anwar, and Fatih Porikli. Underwater scene prior inspired deep underwater image and video enhancement. *Pattern Recognition*, 98:107038, 2020. 6
- [26] Chongyi Li, Chunle Guo, Wenqi Ren, Runmin Cong, Junhui Hou, Sam Kwong, and Dacheng Tao. An underwater image enhancement benchmark dataset and beyond. *IEEE TIP*, 29:4376–4389, 2020. 1, 2, 3, 6, 7, 8, 11
- [27] Chongyi Li, Jichang Guo, Shanji Chen, Yibin Tang, Yanwei Pang, and Jian Wang. Underwater image restoration based on minimum information loss principle and optical properties of underwater imaging. In *ICIP*, pages 1993–1997, 2016. 1, 3
- [28] Chongyi Li, Jichang Guo, and Chunle Guo. Emerging from water: Underwater image color correction based on weakly supervised color transfer. *IEEE Signal. Process. Lett.*, 25(3):323–327, 2018. 1, 2, 3
- [29] Chong-Yi Li, Ji-Chang Guo, Run-Min Cong, Yan-Wei Pang, and Bo Wang. Underwater image enhancement by dehazing with minimum information loss and histogram distribution prior. *IEEE TIP*, 25(12):5664–5677, 2016. 1
- [30] Chong-Yi Li, Ji-Chang Guo, Run-Min Cong, Yan-Wei Pang, and Bo Wang. Underwater image enhancement by dehazing with minimum information loss and histogram distribution prior. *IEEE TIP*, 25(12):5664–5677, 2016. 1, 3

- [31] Jie Li, Katherine A Skinner, Ryan M Eustice, and Matthew Johnson-Roberson. Watergan: Unsupervised generative network to enable real-time color correction of monocular underwater images. *IEEE Robot. Autom. Lett.*, 3(1):387–394, 2017. 1, 2, 3
- [32] Risheng Liu, Xin Fan, Ming Zhu, Minjun Hou, and Zhongxuan Luo. Real-world underwater enhancement: Challenges, benchmarks, and solutions under natural light. *IEEE Trans. Circuits. Syst. Video Technol.*, 30:4861–4875, 2020. 2, 3
- [33] Anish Mittal, Rajiv Soundararajan, and Alan C. Bovik. Making a “completely blind” image quality analyzer. *IEEE Signal Process. Lett.*, 20(3):209–212, 2013. 6
- [34] Karen Panetta, Chen Gao, and Sos Agaian. Human-visual-system-inspired underwater image quality measures. *IEEE J. Ocean. Eng.*, 41(3):541–551, 2016. 3, 6
- [35] Yan-Tsung Peng and Pamela C Cosman. Underwater image restoration based on image blurriness and light absorption. *IEEE TIP*, 26(4):1579–1594, 2017. 1, 3, 6, 7, 8, 11, 13
- [36] Robi Polikar. Ensemble learning. In *Ensemble machine learning*, pages 1–34. Springer, 2012. 3
- [37] Olaf Ronneberger, Philipp Fischer, and Thomas Brox. U-net: Convolutional networks for biomedical image segmentation. In *MICCAI*, pages 234–241. Springer, 2015. 6
- [38] Pooja Sahu, Neelesh Gupta, and Neetu Sharma. A survey on underwater image enhancement techniques. *IJCA*, 87(13), 2014. 1
- [39] Raimondo Schettini and Silvia Corchs. Underwater image processing: State of the art of restoration and image enhancement methods. *EURASIP. J. Adv. Signal Process.*, 2010:1–14, 2010. 1
- [40] Wei Song, Yan Wang, Dongmei Huang, and Dian Tjondronegoro. A rapid scene depth estimation model based on underwater light attenuation prior for underwater image restoration. In *PCM*, pages 678–688. Springer, 2018. 1, 3
- [41] Pritish M Uplavikar, Zhenyu Wu, and Zhangyang Wang. All-in-one underwater image enhancement using domain-adversarial learning. In *CVPR Workshops*, pages 1–8, 2019. 1, 3, 6, 7, 8, 13
- [42] Ashish Vaswani, Noam Shazeer, Niki Parmar, Jakob Uszkoreit, Llion Jones, Aidan N Gomez, Łukasz Kaiser, and Illia Polosukhin. Attention is all you need. In *NIPS*, pages 5998–6008, 2017. 3
- [43] Haonan Wang, Peng Cao, Jiaqi Wang, and Osmar R. Zaiane. Uctransnet: Rethinking the skip connections in u-net from a channel-wise perspective with transformer, 2021. 4
- [44] Yi Wang, Hui Liu, and Lap-Pui Chau. Single underwater image restoration using adaptive attenuation-curve prior. *IEEE Trans. Circuits. Syst. I. Regul. Pap.*, 65(3):992–1002, 2018. 1
- [45] Hung-Yu Yang, Pei-Yin Chen, Chien-Chuan Huang, Ya-Zhu Zhuang, and Yeu-Horng Shiau. Low complexity underwater image enhancement based on dark channel prior. In *IBICA*, pages 17–20, 2011. 1, 3
- [46] Miao Yang, Jintong Hu, Chongyi Li, Gustavo Rohde, Yixiang Du, and Ke Hu. An in-depth survey of underwater image enhancement and restoration. *IEEE Access.*, 7:123638–123657, 2019. 1
- [47] Miao Yang, Ke Hu, Yixiang Du, Zhiqiang Wei, Zhibin Sheng, and Jintong Hu. Underwater image enhancement based on conditional generative adversarial network. *Signal Process., Image Commun.*, 81:115723, 2020. 2
- [48] Miao Yang and Arcot Sowmya. An underwater color image quality evaluation metric. *IEEE TIP*, 24(12):6062–6071, 2015. 3, 6
- [49] Jun-Yan Zhu, Taesung Park, Phillip Isola, and Alexei A. Efros. Unpaired image-to-image translation using cycle-consistent adversarial networks. In *ICCV*, pages 2242–2251, 2017. 2

## A. Overview

This supplementary document provides complimentary details about the LSUI dataset (Sec.B) and comparisons (Sec.C) in the paper. We also provide the comparison of underwater video enhancement results of different underwater image enhancement methods in the supplementary video.

## B. LSUI Dataset

As shown in Fig .7, compared with UIEB [26], our LSUI dataset contains larger number of images and richer underwater scenes and object categories. In particular, our LSUI dataset includes deep-sea scenes and underwater cave scenes that are not available in previous underwater datasets. We provide some examples of our LSUI dataset in Fig 8, which shows that our LSUI dataset contains a variety of underwater scenes, water types, lighting conditions and target categories. As far as we know, LSUI is the largest real underwater image dataset with high quality reference images until now, and we believe it will facilitate the further development of underwater imaging techniques.

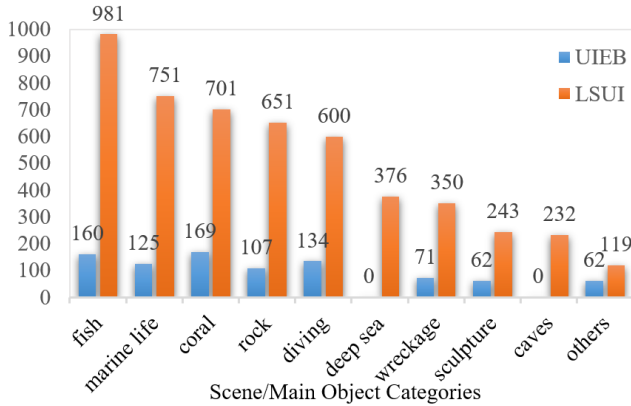


Figure 7. Statistics of our LSUI dataset and the existing largest real underwater dataset UIEB [26] with high quality reference images.

## C. Additional Visual Comparisons

### C.1. Visual Examples of Dataset Evaluation

Fig. 9 is the sampled enhancement results of U-shape transformer trained on different underwater datasets, which is a supplement of the *Data Evaluation* part of the paper. Enhancement results training on Train-L (a portion of our LSUI dataset) demonstrates the highest PSNR value and preferable visual quality, while results training on other datasets show a certain degree of color cast. For the high-quality reference images and rich underwater scenes (lighting conditions, water types and target categories), our constructed LSUI dataset could improve the imaging quality

and generalization performance of the UIE network.

### C.2. Visual Comparisons of Non-Reference Experiments

Fig. 10 is a supplement to the *Non-reference Evaluation* of the paper. Enhancement results of our method have the highest PS value, which index reflects the visual quality. Generally, compared methods are unsatisfactory, which includes undesirable color artifacts, over-saturation and unnatural color casts. Among the methods, results of the UIBLA [35] and FUnIE [19] are collectively reddish and yellowish, respectively. Retinex based [11] method introduces artifacts and unnatural colors. UGAN and UIT-DAL have the issue of local over-enhancement and color artifacts, which main reason is they ignore the inconsistent attenuation characteristics of the underwater images in the different space areas and the color channels. Although Ucolor [24] introduces the transmission medium prior to reinforcing the network’s attention on the spatial area with severe attenuation, it still ignores the inconsistent attenuation characteristics of the underwater image in different color channels, which results in the problem of overall color cast.

### C.3. Visual Comparisons of Full-Reference Experiments

Fig. 11 is a supplement to the *Full-reference Evaluation* of the paper. Results of our method are the closest with the reference images, which have the best visual quality and the highest PSNR value. Five selected methods exhibit a different degree of color artifacts and casts, which enhancement results differ considerably from the object’s original color and fall far short from the reference images. Among the methods, Fusion [2] does not remove the color casts (bias to green) and exhibits severe color artifacts. Retinex based [11] method could improve the image contrast to a certain extent, but the color of the enhanced image is unnatural. The enhancement result of FUnLE [19] is yellowish overall. Although UGAN [9] and Ucolor [26] could provide relatively good color appearance, they are often affected by local over-enhancement, and there are still some color casts in the results. The limitation of the UGAN and Ucolor method is that their network structures do not consider the inconsistent attenuation of underwater images in different color channels and spatial regions.

### C.4. Visual Comparisons of Ablation Study

As shown in Fig .12, the enhancement result of the full model has the highest PSNR score and best visual quality. The results of BL+MSG have less noise and artifacts than that of the single BL module, which is due to the mechanism of MSG helps to reconstruct local details. The results’ overall color of BL+MCSL are close to the reference picture for which adds a multi-color space loss function. How-



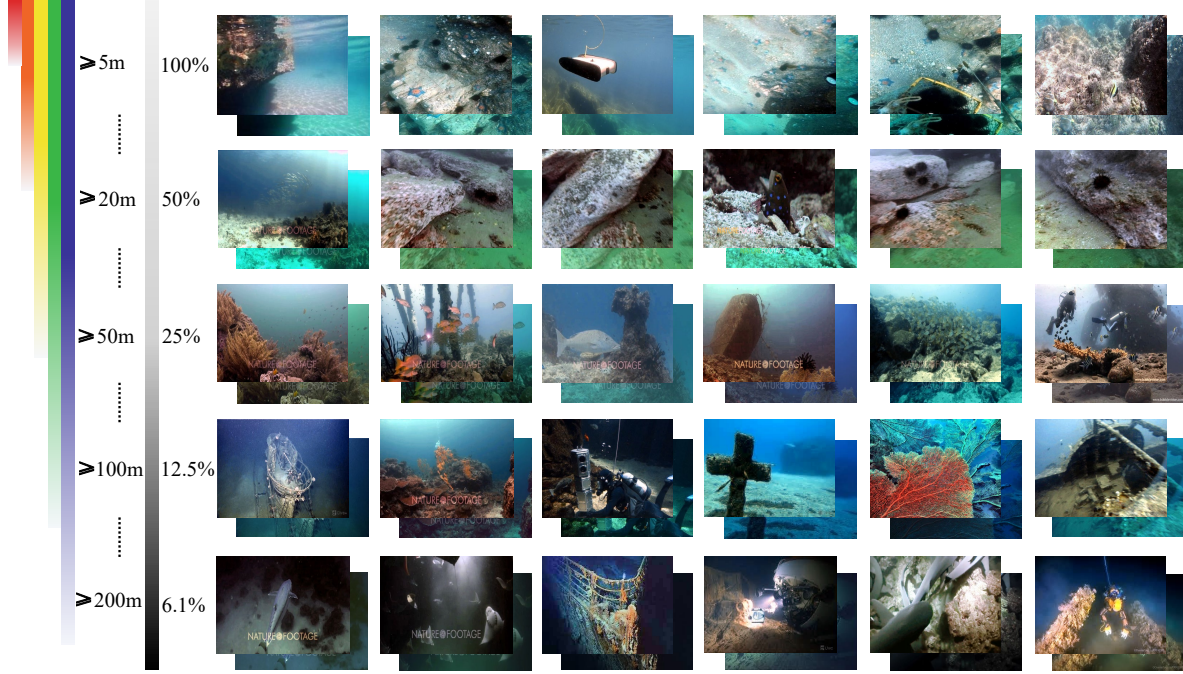


Figure 8. Example images in the LSUI dataset. The top of each pair of images is the reference image, and the bottom is the raw underwater image.

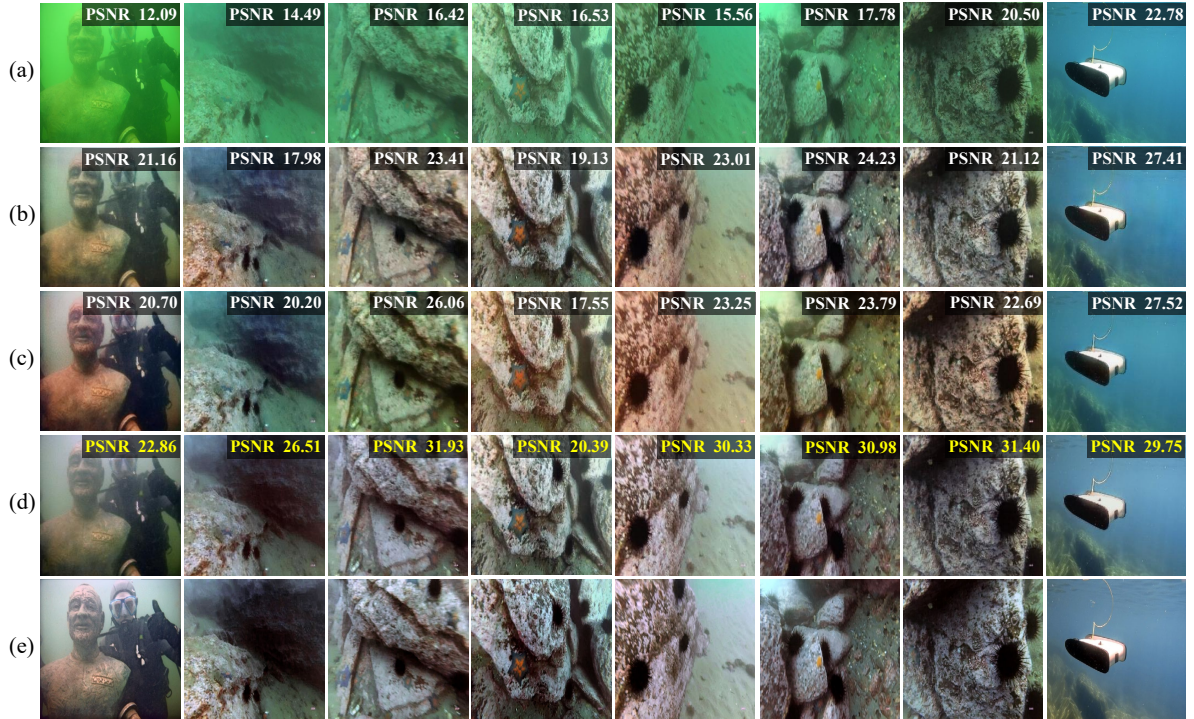


Figure 9. Enhancement results of U-shape transformer trained on different underwater datasets. (a): Input images sampled from Test-L504; (b): Enhanced results using the model trained on the Train-U; (c): Enhanced results using the model trained on the Train-E; (d): Enhanced results using the model trained by our proposed dataset Train-L; (e): Reference images(recognized as ground truth (GT)).



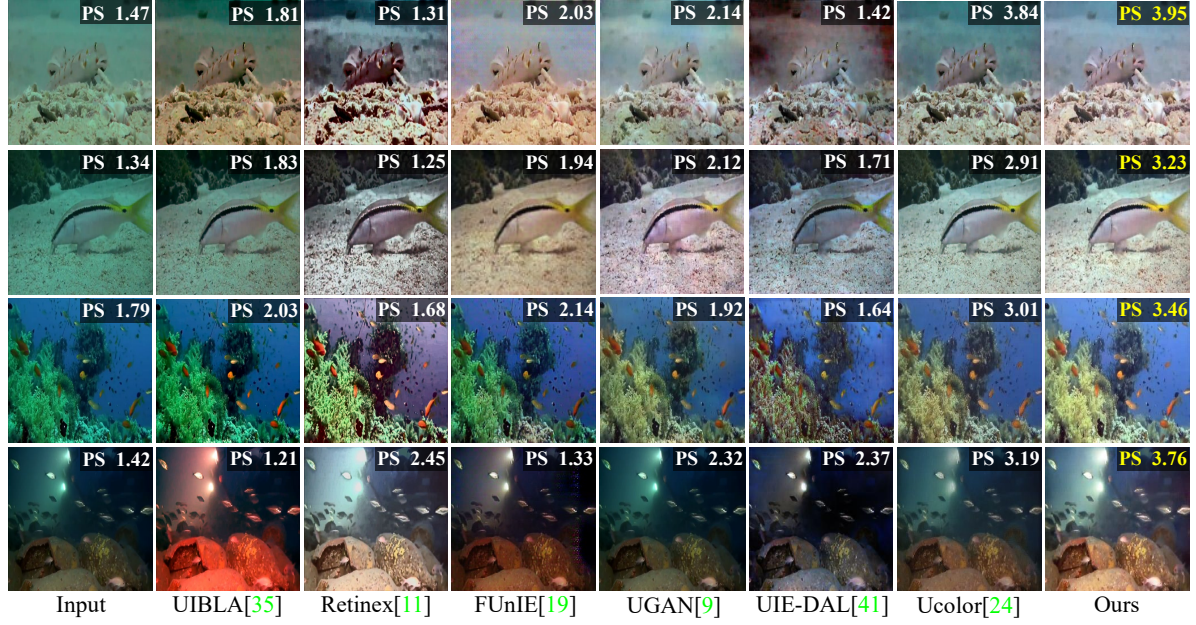


Figure 10. Visual comparison sampled from the Test-U60 dataset. From left to right are raw images, results of UIBLA [35], Retinex based [11], FUnIE [19], UGAN [9], Ucolor [24], UIE-DAL [41] and our U-shape Transformer.

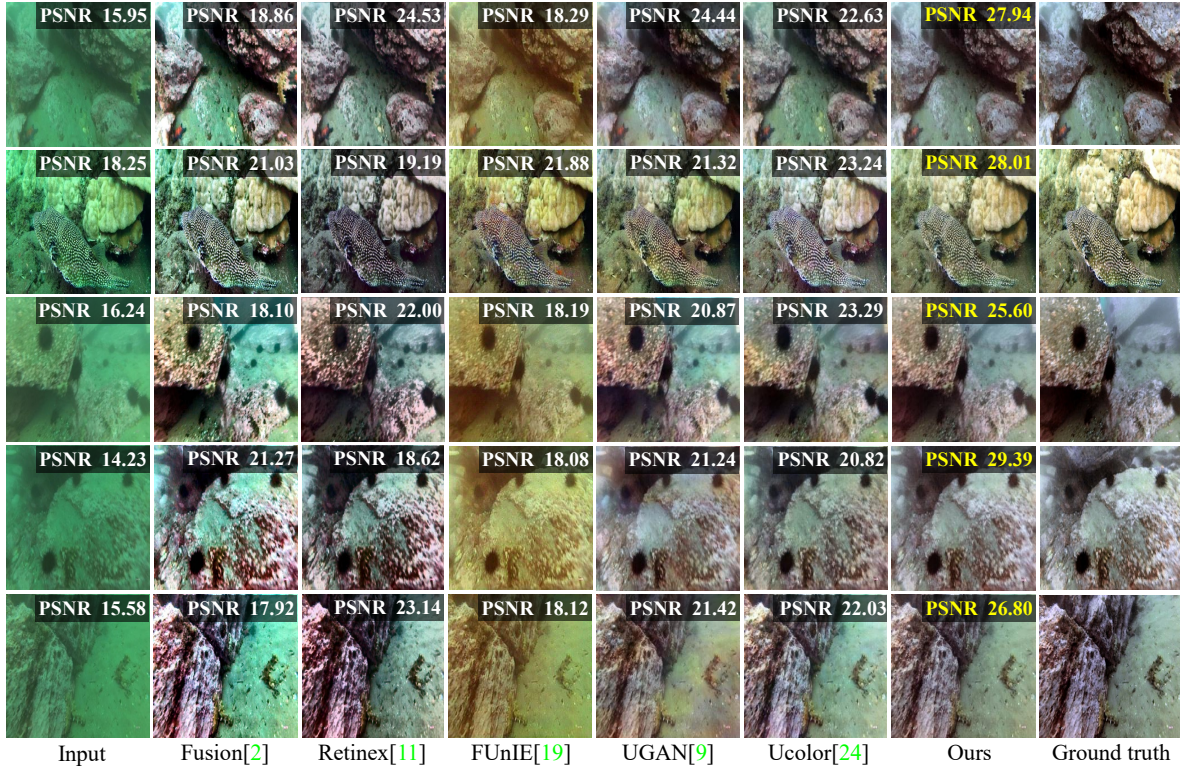


Figure 11. Visual comparison of enhancement results sampled from the Test-L504 dataset. From left to right are raw images, results of Fusion [2], Retinex based [11], FUnIE [19], UGAN [9], Ucolor [24], our U-shape Transformer and the reference image (recognized as ground truth (GT)).

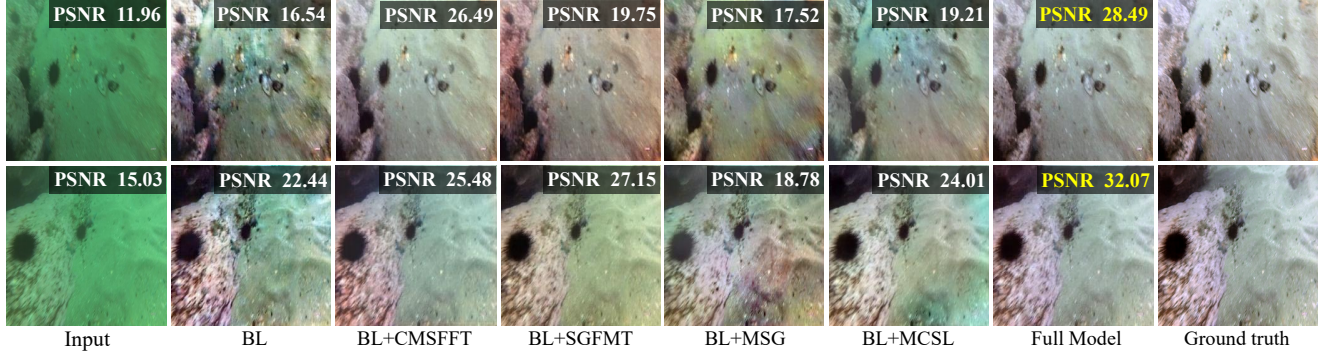


Figure 12. Visual comparison of the ablation study, which images are sampled from the Test-L504 dataset. The highest PSNR score is marked in yellow.

ever, the unevenly distributed visualization and artifacts in local areas of BL+MCSL are owing to the absence of attention mechanism guidance. Although the enhanced results of BL+CMSFFT and BL+SGFMT are evenly distributed, the overall color is not accurate. The investigated four modules have their particular functionality in the enhancement process, which integration could improve the overall performance of our network.